

Reviewer 2

The authors appreciate the reviewer's evaluation and detailed valuable comments. We tried our best to address all the raised issues and revise the paper accordingly. What follows is a point-by-point reply to the comments and the proposed modification. As some of the raised points are close to the comments of the 1st respected reviewer, there are similarities in the following replies and corresponding actions with the previously uploaded file (RC1).

To facilitate following the comment sheet, comments and the responses are printed in blue font and black italic font, respectively. We hope the reviewer accepts the revisions and supports our revised paper merits the review process in Ocean Science.

Yours sincerely,

S. Mahya Hoseini

Mohsen Soltanpour

The paper presents a study of the tidal characteristics of the Persian Gulf and on the influence of Coriolis forces, bathymetry, and bottom friction on its propagation. The authors present a validation of the model and discuss the numerical model results and those obtained for an idealized case. The authors claim that the “tidal modelling in the Persian Gulf needs improving despite previous efforts with comparisons to new water levels...”, however this new data covers the same period that the other studies they cite. The novelty of the study is not clear enough in the current manuscript and it is not clear that this model performs better than the one followed by other studies that the cite e.g. Ranji and Soltanpour since no comparisons are provided. The manuscript will also benefit of clarifications at some points. I cannot recommend the publication of this paper. Below I provide some more comments that hopefully will help in future submissions.

Thank you for your comments. The goal of the present research was to study the physics of tide in the PG. As we wrote in the first sentence of the abstract (i.e., 2D hydrodynamic model is employed to study the characteristics of tidal wave propagation in the Persian Gulf), the hydrodynamic model was only used as a tool, alongside other methods such as the analysis of field measurements and propagation of Kelvin wave, for understanding the dynamics of the tide in the PG.

We acknowledge that our employed model has similarities with the numerical model of recently published study of Ranji and Soltanpour (2021). They proposed a general method, which was tested in the PG as a case study, for the spatial optimization of the Manning coefficient, as a function of water depth, mean velocity, vegetation, and bed sediment size, to increase the performance of 2D hydrodynamic modeling. Fig. R1 presents the final results of their optimization process, which resulted in slight overall improvement of model outputs of about 3%, compared to applying a constant friction. It is observed that although a maximum improvement of 27.5% is obtained at Khuran Channel, the accuracy of predictions decreased at the southern PG coastline and near the islands, e.g., - 8% changes at Bahrain Station. The poor performance at the shallow water stations was related to the lack of good quality bathymetry data.

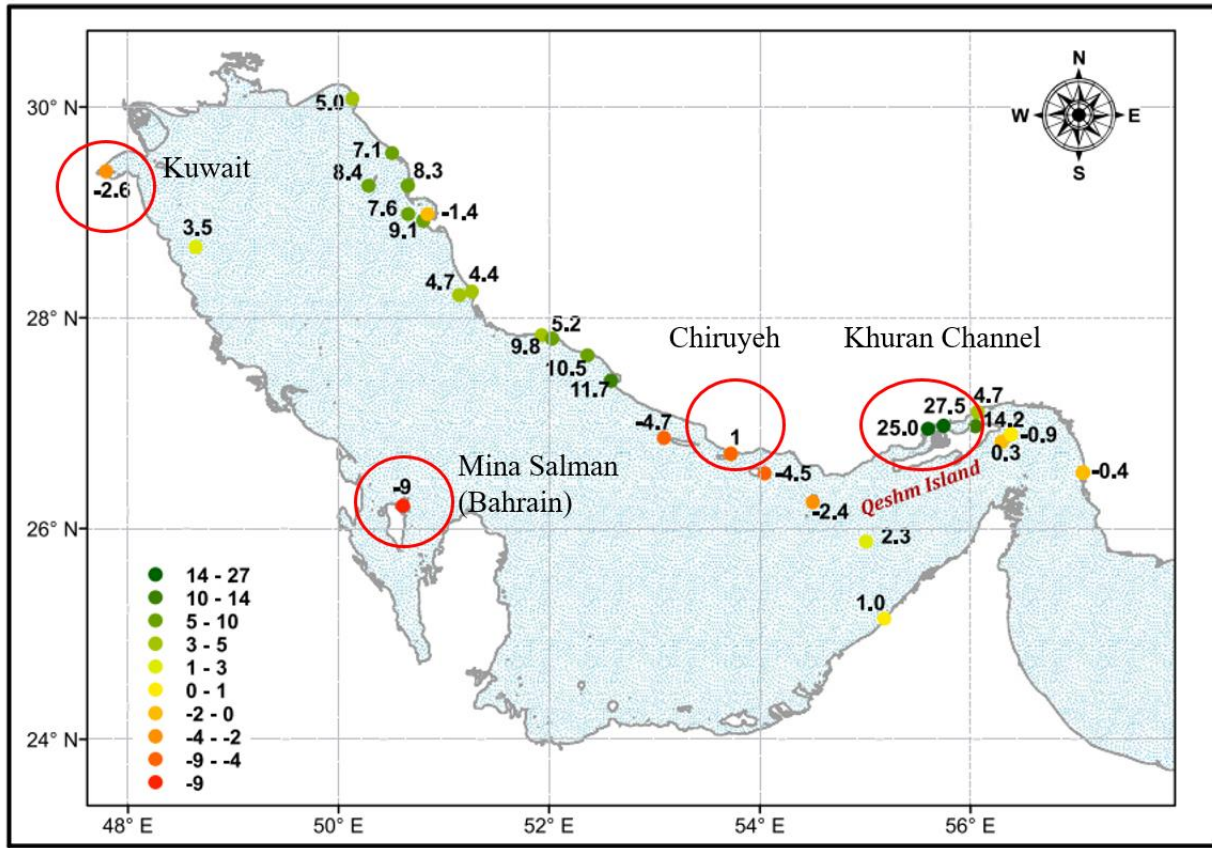


Fig. R1: Changes of objective functions at different stations for spatially varying bottom friction versus the fixed Manning number (Ranji and Soltanpour, 2021).

It should also be added that unlike Ranji and Soltanpour's (2021) model that was only verified by water level measurements, here the numerical model was also compared with tidal constituents of UKHO, and current speeds at different locations.

The verified model was then employed to study the tidal wave characteristics and its propagation in the PG. This is the main objective of present study, which is different from the past studies. The analysis of field data at north coastline of the PG is also new in this research (figure 4, page 7). A series of numerical tests was also conducted to investigate the various effects of PG geometry, PG bathymetry, Coriolis force, and bed friction on tidal wave propagation (Section 4: Discussions on tidal wave propagation, pages 23-32).

The following list can be considered as the innovations of the present research:

- Study of the effects of the governing factors, i.e., geometry and bathymetry, Coriolis force, and bed roughness, on tidal wave propagation in the PG by a series of numerical tests (section 4, pages 23-32).*
- The tide in the PG is represented by two Kelvin waves traveling in opposite directions, as the result of co-oscillation with the tide in the Gulf of Oman (section 3.3.1, pages 16-17).*
- Study of the effect of the Coriolis force on the tidal regime in the PG, which results in the generation of two amphidromic systems for M_2 and S_2 and one amphidromic system for K_1 and O_1 (section 4.1, pages 24-26).*
- Study of natural oscillation period of PG (mainly diurnal), based on numerical simulations (section 3.3.4, pages 21-22).*
- Presenting the map of tidal constituents on the northern coastline of the PG (figure 4, page 7), based on field measurements and the maps of shallow-water constituents (figure 16, page 20) and maximum tidal amplitudes (figure 19, page 23) in the PG, based on model results.*

As our field measurements is not the same as employed data of other researches, it is not possible to directly compare the performance of present model and past published modeling studies. However, the present modeling might be advantageous to previous ones because of the large employed data set for its verification, i.e. water levels, current speeds and tidal constituents at different locations of PG. The high-resolution bathymetry data on the north coast of the PG (figure 5) is another favorable component of present model, which has only been used in Ranji and Soltanpour (2021).

As it was discussed above, the present model has similarities with the numerical model of Ranji and Soltanpour (2021). Figure R2 shows the comparisons between the present model and the model of Ranji and Soltanpour (2021), before the optimization process. It is observed that the accuracy of both models is approximately the same. Using spatially varying Manning coefficient, their optimization process resulted in higher correlations in some stations and more discrepancies in some other with an overall better performance of about +3%, compared to applying a constant friction (please refer to Fig. R1). It should be added that wind force was also included in the driving forces of the model of Ranji and Soltanpour (2021). The poor model performances at Bahrain (Mina Salman) can be related to the low accuracies of both general bathymetry data, i.e. ETOPO2v2 (present study) and GEBCO (Ranji and Soltanpour, 2021), in shallow areas of south PG.

Considering that the present model does not prove to be superior to Ranji and Soltanpour's (2021) model and to accommodate this comment, the following sentence will be omitted from the revised manuscript:

“Despite all past efforts, tidal modeling in the PG still needs to be improved, with comparisons to new water levels and current speeds measurements at different locations.”

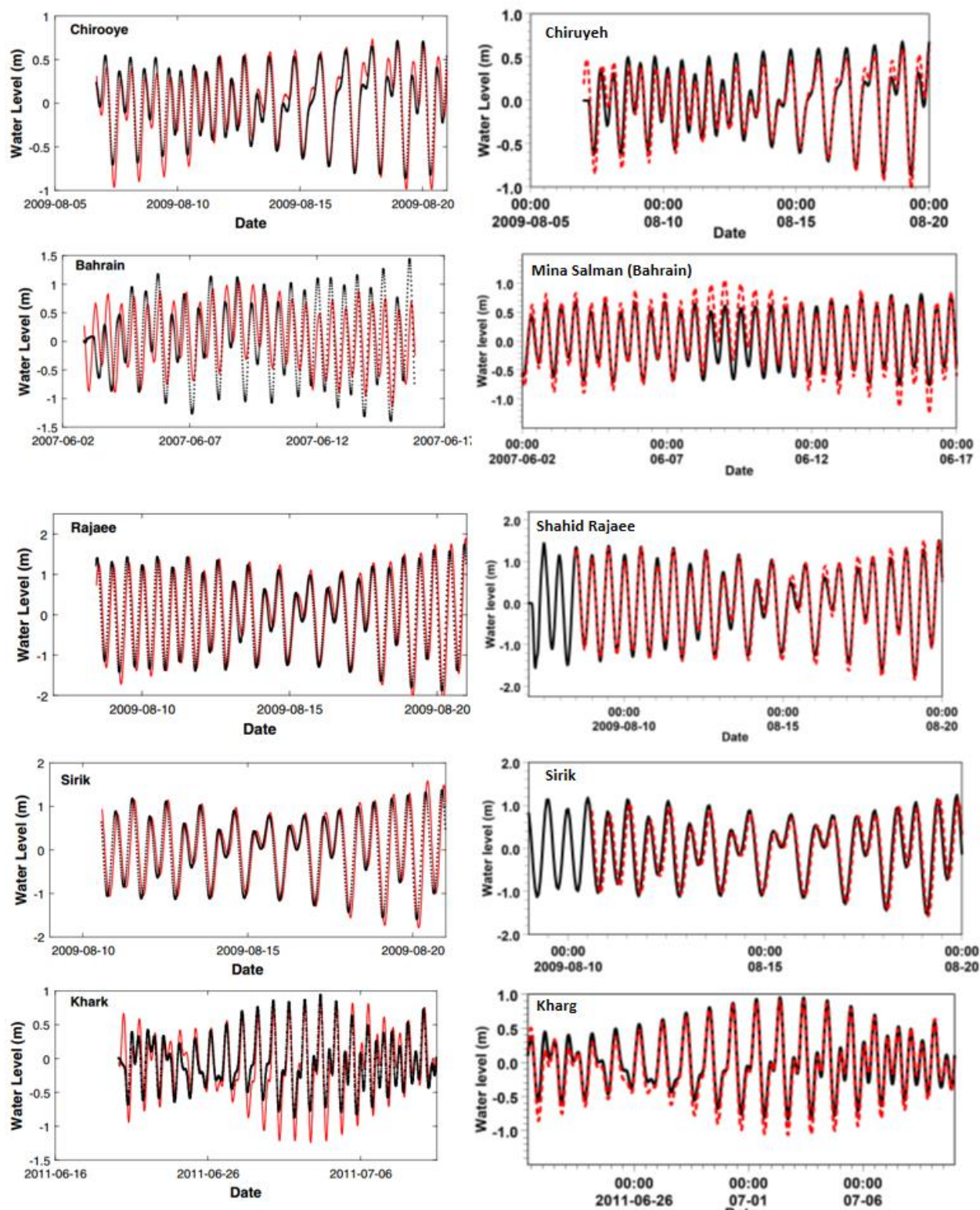


Fig. R2: Comparisons of water levels at selected stations. Red and black lines respectively present the field data and models (Left: Ranji and Soltanpour, 2021, Right: present study).

The description of the model can be improved. The information on how the model is forced is buried at the end of the section and the way bottom friction is considered is not very clear. It may be clearer to present the model first and then the sensitivity tests performed on the position of the open boundary and the Manning coefficient.

Thank you for the comment. The structure of “Numerical model” will be modified including the new section “3.1 Governing equations” (page 7, line 124) as follows:

3 Numerical model

3.1 Governing equations

3.2 Model setup

3.2.1 Bathymetry and computational grid

3.2.2 Open boundary

3.2.3 Bed friction

3.1 Governing equations

Forcing the water level at the open boundary, Flow Model (FM) of MIKE 21 (DHI, 2012) is used for the 2D hydrodynamic simulation of the PG. The continuity and momentum equations are:

$$\frac{\partial h}{\partial t} + \frac{\partial h\bar{u}}{\partial x} + \frac{\partial h\bar{v}}{\partial y} = hS \quad (1)$$

$$\begin{aligned} \frac{\partial h\bar{u}}{\partial t} + \frac{\partial h\bar{u}^2}{\partial x} + \frac{\partial h\bar{u}\bar{v}}{\partial y} &= f\bar{v}h - gh\frac{\partial\eta}{\partial x} - \frac{1}{\rho_w}\frac{\partial P_a}{\partial x} - \frac{gh^2}{2\rho_w}\frac{\partial\rho}{\partial x} + \frac{\tau_{sx}}{\rho_w} - \frac{\tau_{bx}}{\rho_w} - \frac{1}{\rho_w}\left(\frac{\partial S_{xx}}{\partial x} + \right. \\ &\left. \frac{\partial S_{yy}}{\partial y}\right) + \frac{\partial}{\partial x}(hT_{xx}) + \frac{\partial}{\partial y}(hT_{xy}) + hu_sS \\ \frac{\partial h\bar{v}}{\partial t} + \frac{\partial h\bar{v}\bar{u}}{\partial x} + \frac{\partial h\bar{v}^2}{\partial y} &= -f\bar{u}h - gh\frac{\partial\eta}{\partial y} - \frac{1}{\rho_w}\frac{\partial P_a}{\partial y} - \frac{gh^2}{2\rho_w}\frac{\partial\rho}{\partial y} + \frac{\tau_{sy}}{\rho_w} - \frac{\tau_{by}}{\rho_w} - \\ &- \frac{1}{\rho_w}\left(\frac{\partial S_{yx}}{\partial x} + \frac{\partial S_{yy}}{\partial y}\right) + \frac{\partial}{\partial x}(hT_{xy}) + \frac{\partial}{\partial y}(hT_{yy}) + hv_sS \end{aligned}$$

where t is the time; x and y represent the Cartesian coordinates, η presents the surface elevation, h stands for the still water depth, $H = h + \eta$ is the total water depth, \bar{u} and \bar{v} are depth-averaged velocities in the x and y direction, respectively, P_a is the atmospheric pressure, S is the magnitude of the discharge due to point sources, u_s and v_s respectively present the velocity by which the water

is discharged into the ambient water, and the lateral stresses T_{ij} include viscous friction, turbulent friction and differential advection. The constants are the Coriolis parameter $f = 2\omega \sin\varphi$ as (ω is the angular velocity of the earth's rotation and φ the latitude), the gravitational acceleration g , and the water density ρ_w (DHI, 2012).

Bottom stress in FM is determined as quadratic friction law ($\frac{\tau_b}{\rho_w} = c_d \overline{u_b} |\overline{u_b}|$, c_d : drag coefficient, $\overline{u_b}$: depth-average velocity) and the drag coefficient can be obtained from Manning number ($c_d = \frac{g}{(MH^{\frac{1}{6}})^2}$, M : Manning number, H : water depth) (DHI, 2012). Proper determination of Manning number is important for the accurate hydrodynamic modeling.

The boundary conditions were briefly discussed in page 12, lines 170-172. Open boundary condition in the MIKE 21 Flow Model can be chosen between two combinations of boundary inputs:

1. *Specification of water level and the direction of the flow.*
2. *Specification of a flux boundary as either discharge, flow flux, or Rating curve through the boundary and the flow direction.*

Following the first combination, here the water level was imposed along the line open boundary with the flow direction perpendicular to the boundary. The water level, composed of thirteen tidal constituents (M_2 , S_2 , N_2 , K_2 , K_1 , P_1 , Q_1 , O_1 , M_4 , MS_4 , MN_4 , P_1 , MM , and MF), were extracted from the TPXO8 global tide model at the two end points of the open boundary (Egbert and Erofeeva, 2002). The input values at the grid points along the boundary is interpolated between the two end points by MIKE 21.

Considering the resolution of TPXO8, i.e. 1/6 degrees (<https://www.tpxo.net/global/tpxo8-atlas>), we also checked the extraction of eight points along the open boundary but the change of the results were unnoticeable, in comparison of using the two end points. This can be related to the short length of the boundary, i.e. 1.88 degrees, in comparison to TPXO8 resolution, and deep water depth at that location.

The following explanations will be added to the revised manuscript (page 12, line 170):

Following Ranji et al. (2016), TPXO global tide model is selected to define the water level at the **line open boundary** (Egbert and Erofeeva, 2002) **with the flow direction perpendicular to the boundary**. Thirteen tidal constituents (M_2 , S_2 , N_2 , K_2 , K_1 , P_1 , Q_1 , O_1 , M_4 , MS_4 , MN_4 , P_1 , MM , and

MF) are used to simulate the tide elevations by TPXO8. Constituents are extracted for the two end points of the open boundary and the input values at the grid points along the boundary are interpolated between these end points.

The following sentence will also be added to the manuscript for the clarification of calibrating Manning coefficient (page 10, line 145):

Three Manning coefficients are checked for the sensitivity analysis.

The period of validation seems too short (i.e. about 9 days). The authors do not show that the spring and tide cycle is accurately reproduced. According to Table 1, the authors should have tide gauge data available to provide a longer validation period.

Thank you for the comment. The validation periods for all stations, except Kuwait and Ruwais where limited duration of data is available, was extended to 14 days to cover parts of the neap and spring tides. One complete lunar month of 29 days was not selected to be able to present the whole figure in two pages.

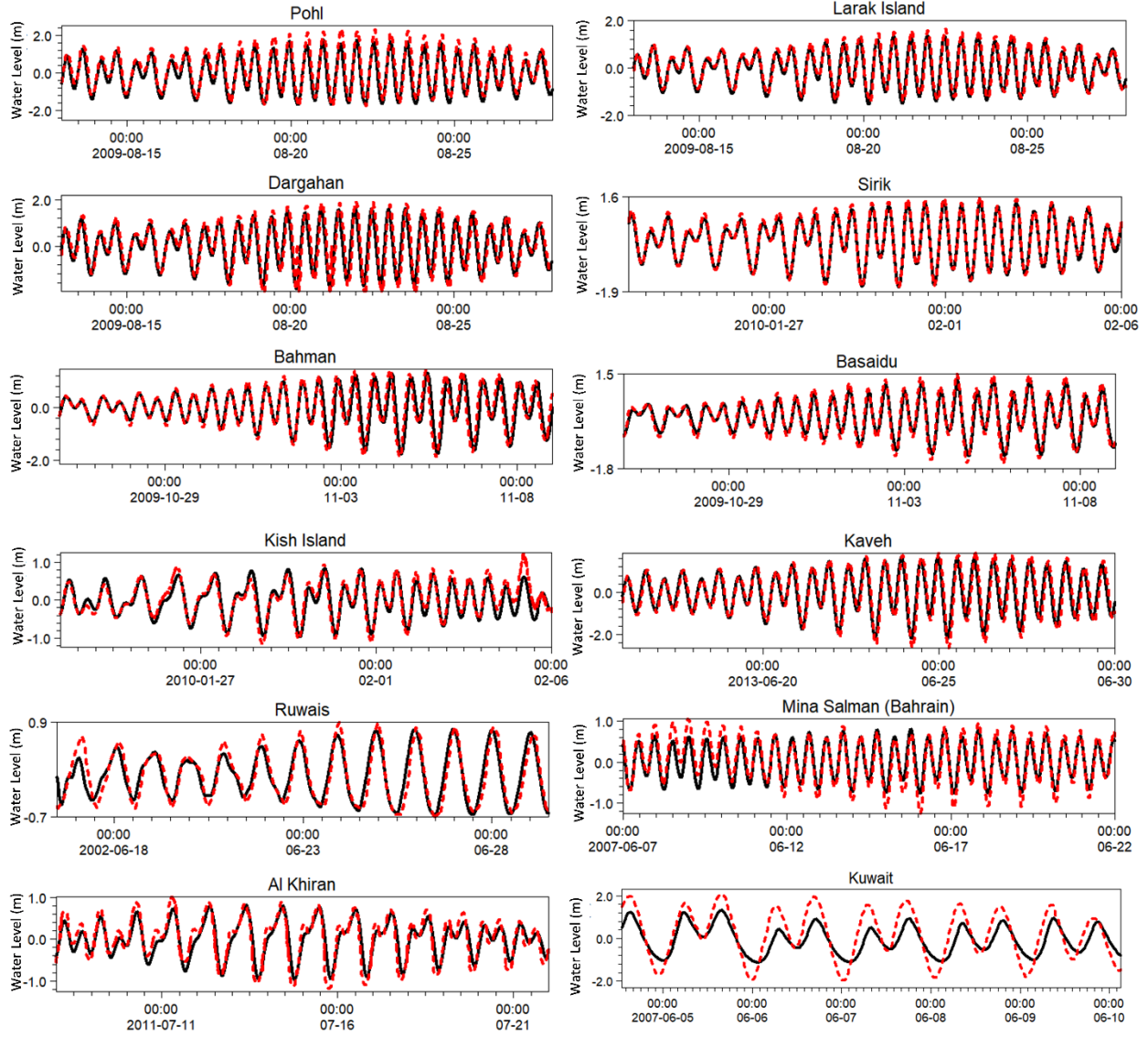


Fig. R3: Comparison of simulated (solid-line) and measured (dash-line) water levels.

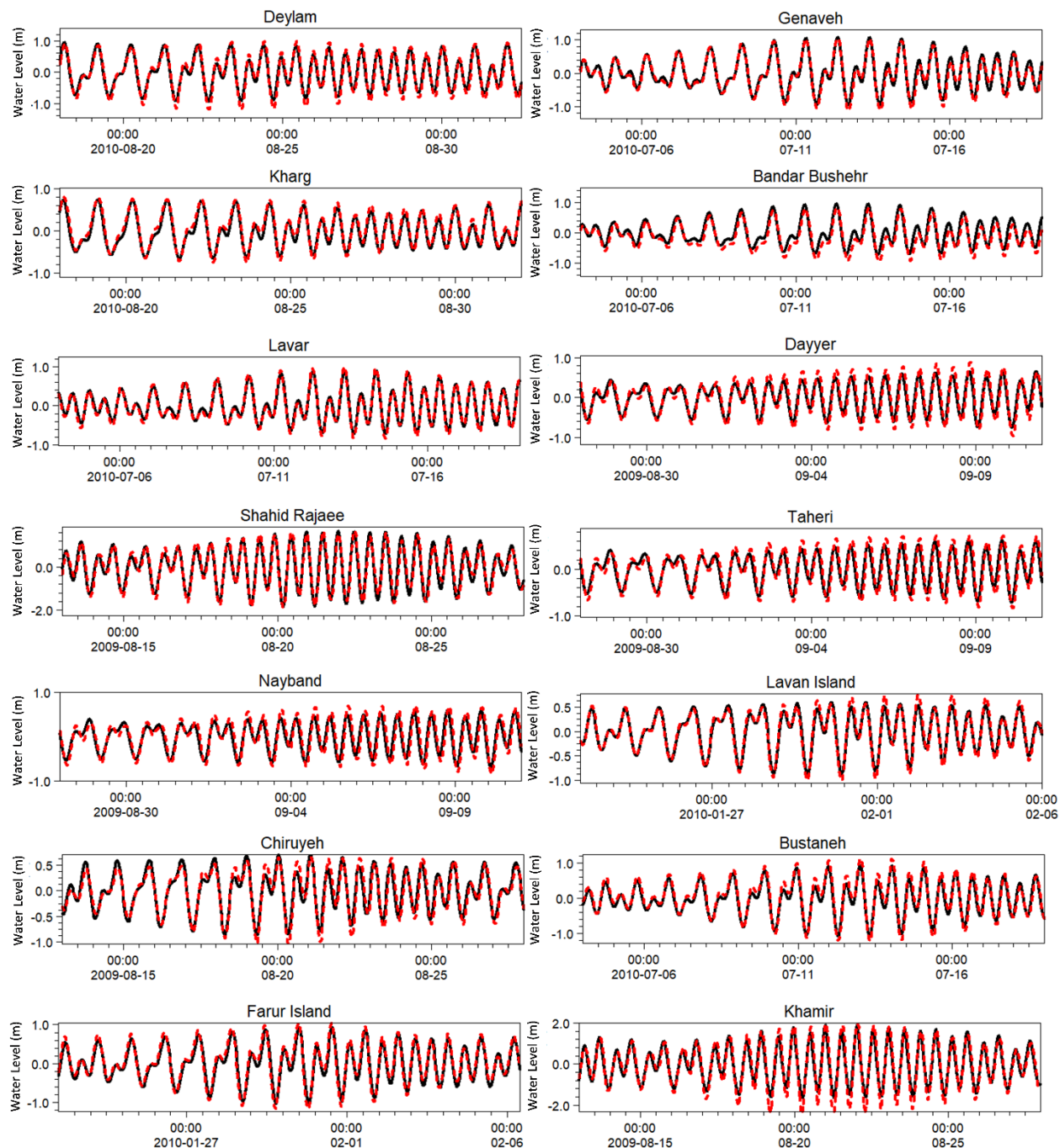


Fig. R3: Comparison of simulated (solid-line) and measured (dash-line) water levels (continued).

There are 28 figures, which seems excessive. Some figures could be combined together (e.g. Figure 1 and Figure 6) and others are probably not necessary (e.g. 5)

Thank you for the comment. We combined figures 2 and 3 into Fig. R4 but it might be better to keep the original figures for the clear visualization of all stations. Figures 5, 6, and 7 were combined into Fig. R5 and figures 12 to 15, 16-17, 21-22, 23-24, and 27-28 were merged together, i.e. Figs. R6 to R10. Thus, the number of figures will be reduced to 18.

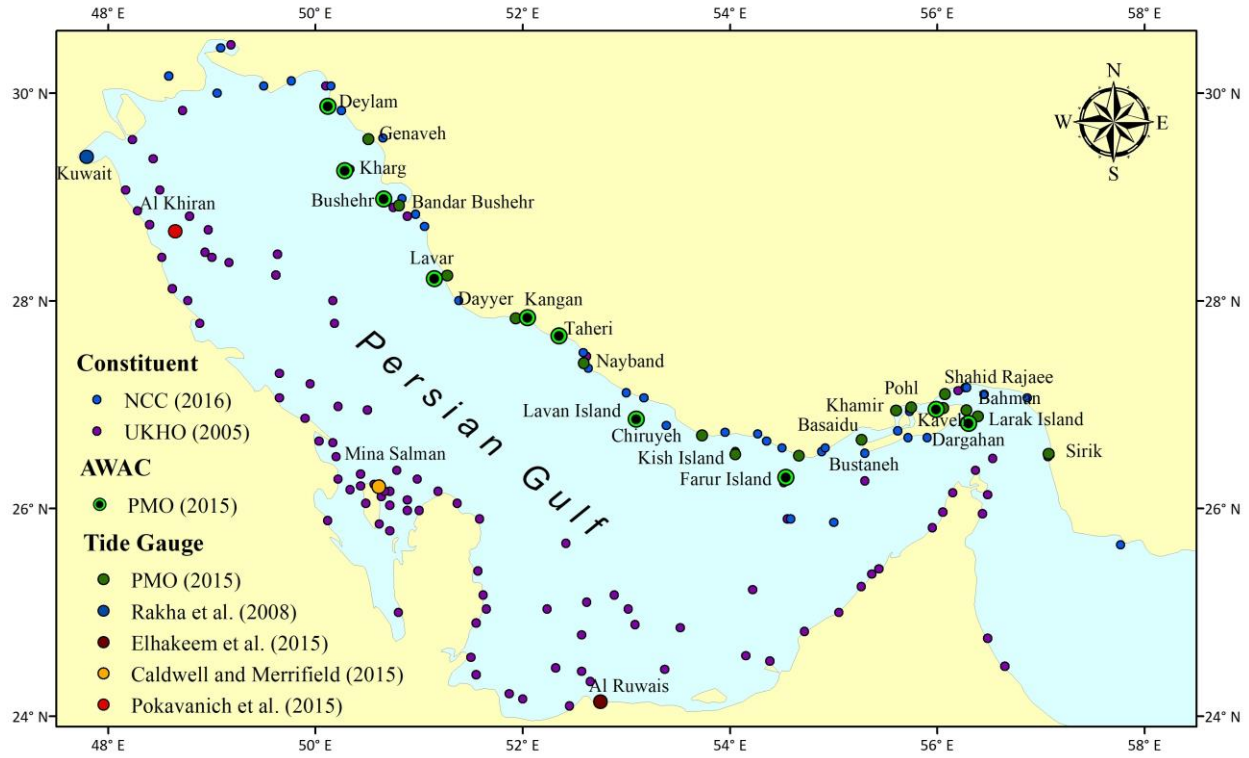


Fig. R4: Water level measurements and harmonic constituent data around the PG.

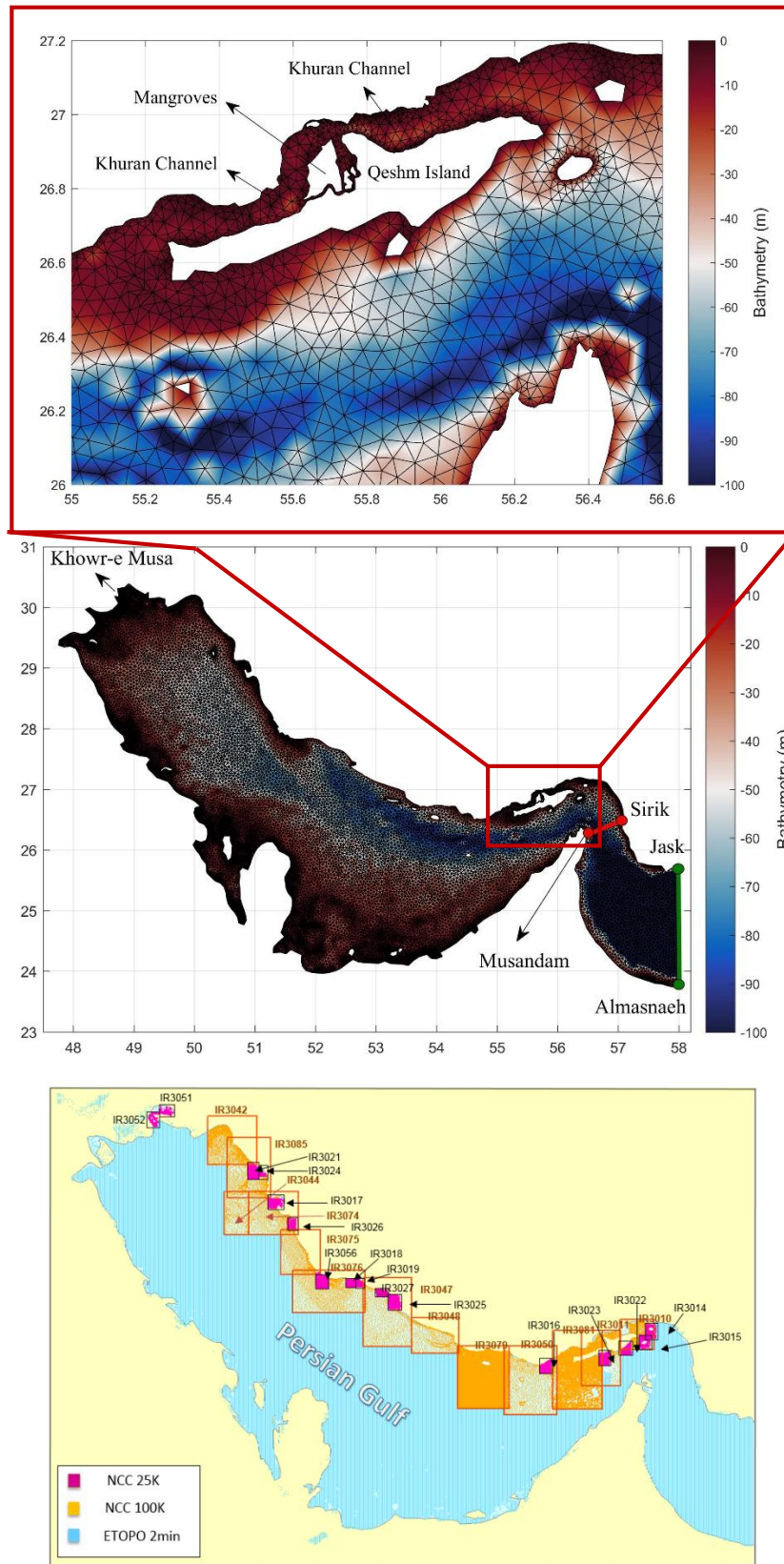


Fig. R5: Computational grid (top and middle) and bathymetry data sources from ETOPO and NCC (bottom). Two alternative locations of open boundary of the model is also presented in middle panel.

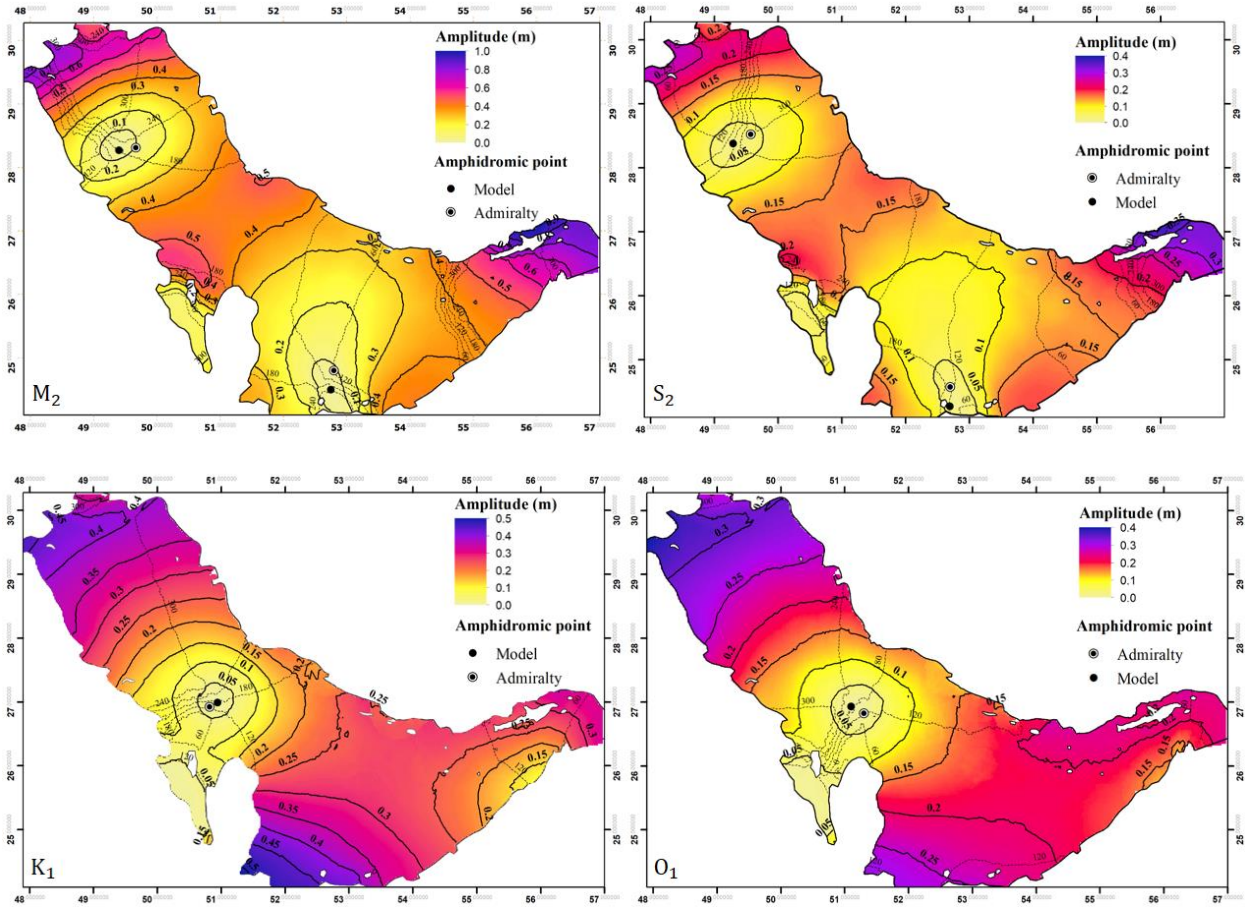


Fig. R6: Simulated co-tidal and co-range charts of principal semidiurnal and diurnal constituents. Solid lines denote co-amplitude lines and dash lines denote co-tidal lines.

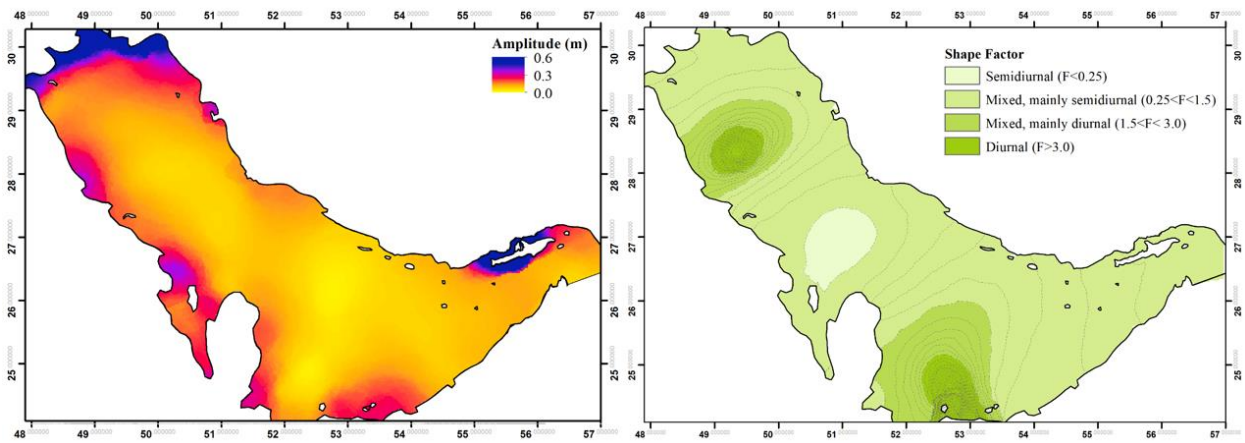


Fig. R7: Map of shallow-water constituents (left) and classification of tides (right) in the PG.

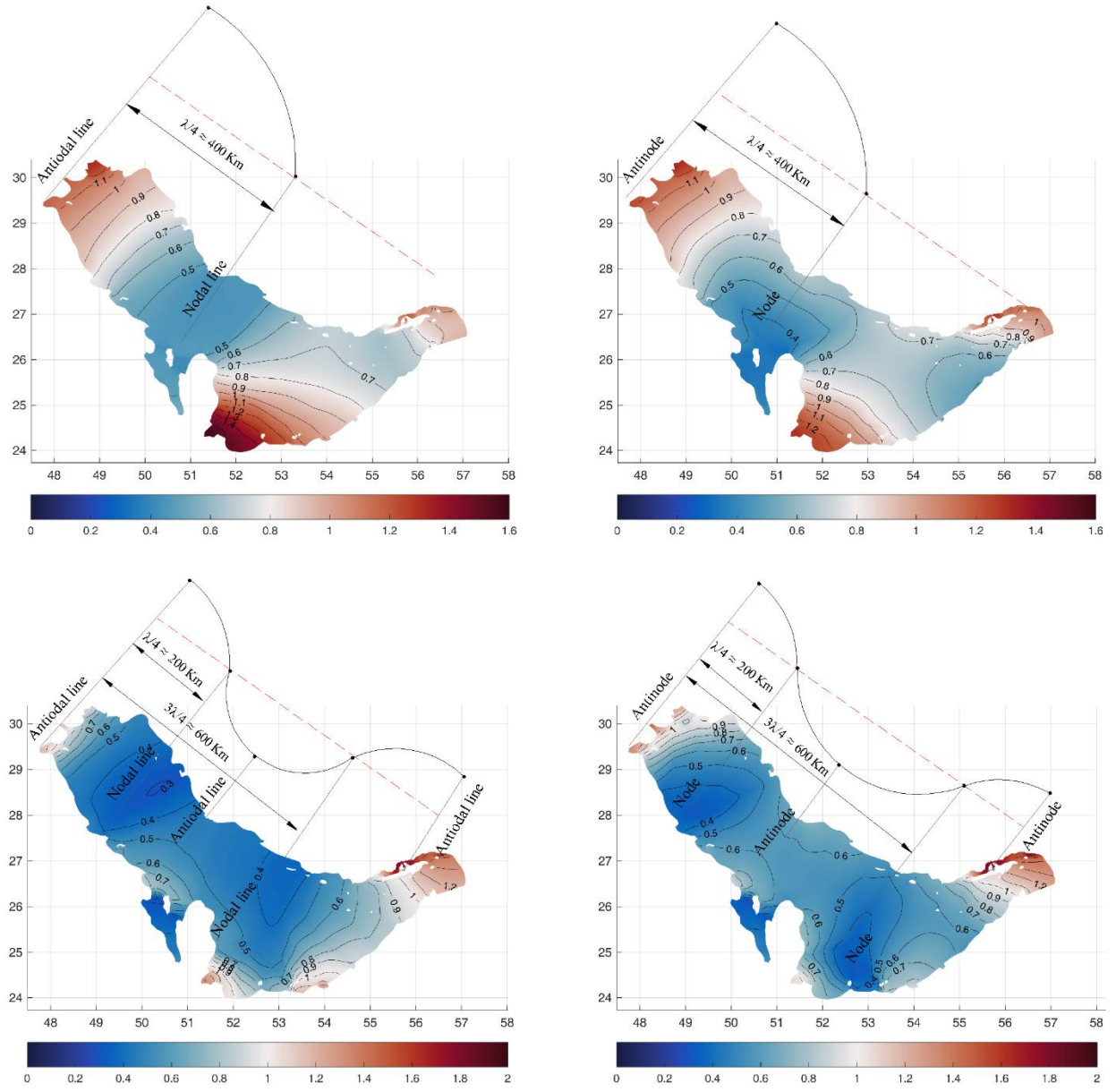


Fig. R8: The locations of the nodal lines and nodes for constituents with the Coriolis force (diurnal: top right, semidiurnal: bottom right) and excluding the Coriolis force (diurnal: top left, semidiurnal: bottom left).

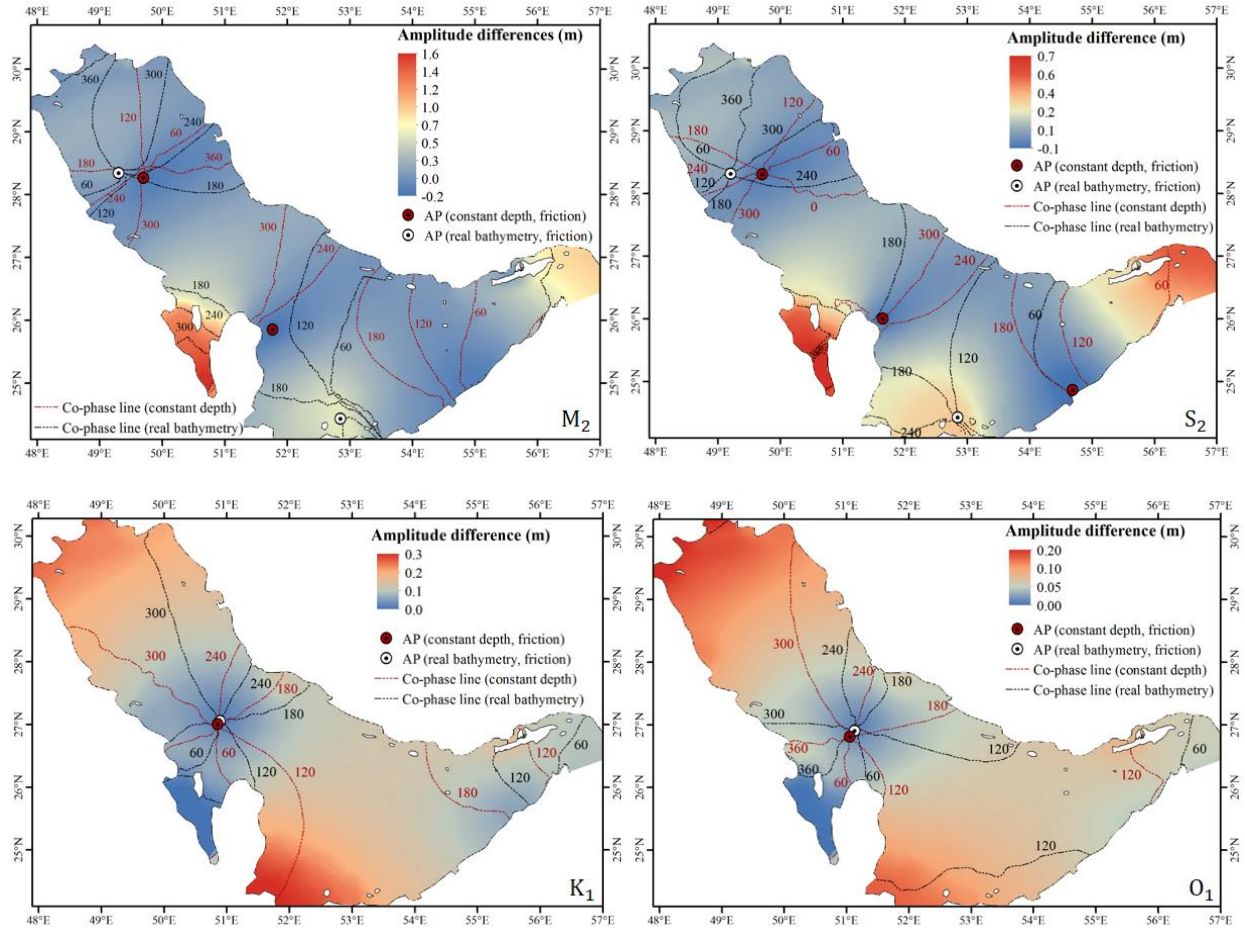


Fig. R9: Co-tidal charts of principal semidiurnal and diurnal constituents, derived from model results in two scenarios including the constant water depth of 36 m and real bathymetry of PG. The background colors show amplitude differences in the two tests.

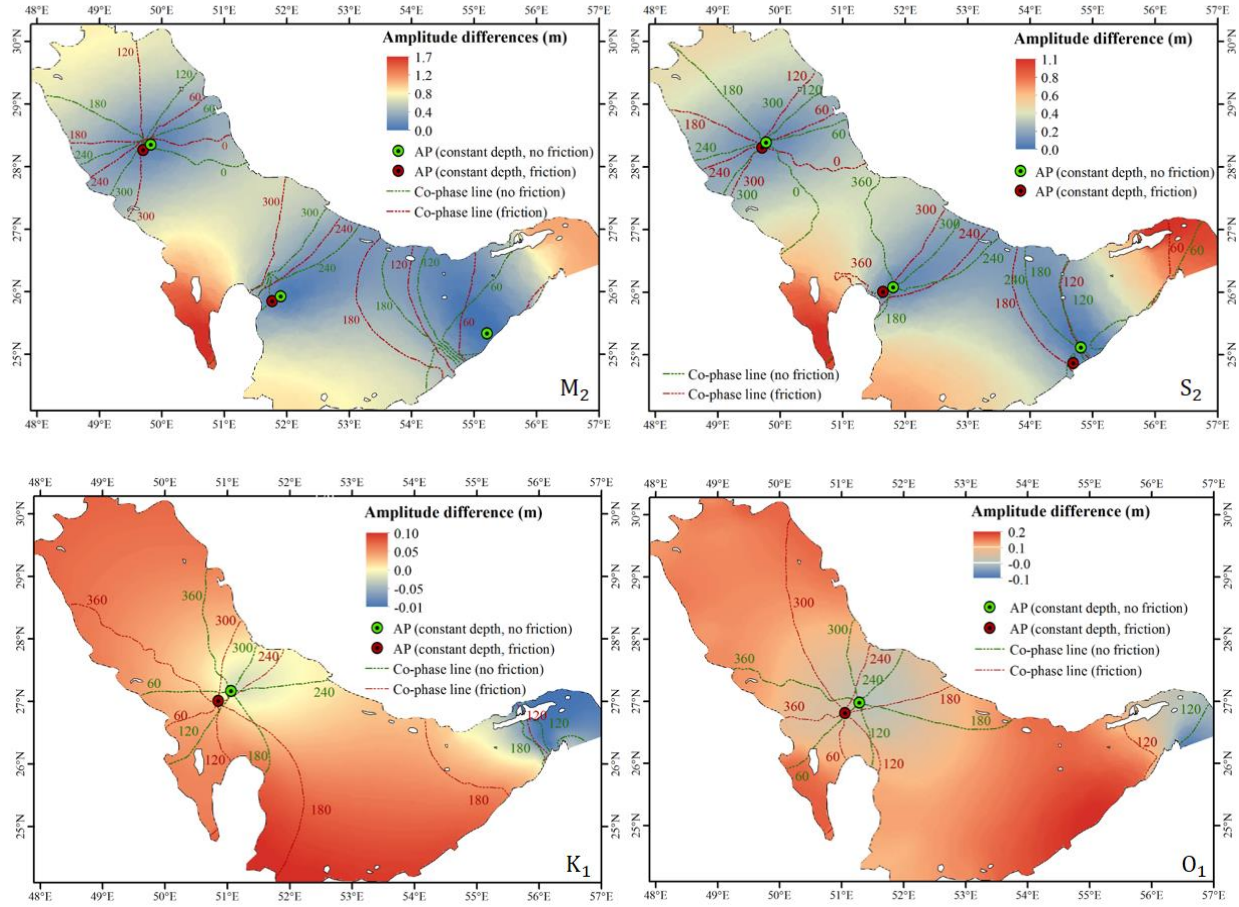


Fig. R10: Co-tidal charts of principal semidiurnal and diurnal constituents with constant water depth of 36 m in two scenarios with and without bed friction. The background colors show the differences of tidal wave amplitudes in the two cases.

I am a bit confused by the results presented since some figures lack an explanation of how they were derived (i.e. Fig. 4, Fig. 20, Fig. 25, Fig. 26) or about why those stations or data are chosen and not others (e.g. Fig. 9).

Thank you for the comment. Figure 4 was generated out of the field measurements by the authors. Please kindly refer to the explanations in pages 6-7, lines 110-120. This definition will be moved to the previous paragraph in the modified manuscript.

Figures 20, 25, and 26, respectively discussed in the sections 4.1, 4.2, and 4.3, were schematically drawn by the authors. For better clarification, this will be mentioned in the revised manuscript (page 24, line 311; page 28, line 370; page 30, line 394):

Figure 20 **schematically** shows the rotational effect of the Coriolis force on two hypothetical rectangular gulfs with intermediate width, located in the northern hemisphere. It is observed that

the Coriolis force results in one AP at $\lambda/4$ from the head of the gulf ($L < 3\lambda/4$, where L is the length of the gulf), and two APs at $\lambda/4$ and $3\lambda/4$ from the head of the gulf ($L > 3\lambda/4$).

Figure 25 **schematically** shows the aforementioned explanations in a hypothetical rectangular gulf located in the northern hemisphere.

Figure 26 **schematically** illustrates this phenomenon in a hypothetical rectangular gulf, located in the northern hemisphere.

Figure 8 that presents the time series of simulated and measured water levels of all the stations but a number of them were shown in Figs. 9 and 11 to limit the size of these figures. To accommodate this comment, Table 4 was completed and Figure 11 was modified by adding the missing data of current measurements.

Table R1: Field measurements (PMO, 2015).

Station	Instrument (Depth, m)	Measurement Period		Station	Instrument (Depth, m)	Measurement Period	
		Start	End			Start	End
Deylam	AWAC (15)	2010/07/09	2010/07/09	Kish Island	TG (3.5)	2010/01/02	2010/04/14
Deylam	TG (3)	2010/07/11	2011/08/11	Farur Island	AWAC (25)	2009/09/10	2010/10/12
Genaveh	TG (3)	2010/06/25	2011/08/20	Bustaneh	TG (4)	2009/11/25	2010/08/18
Kharg	AWAC (25)	2010/ 07/31	2011/07/29	Basaidu	TG (5)	2009/10/22	2009/12/25
Bandar Bushehr	TG (3)	2010/06/24	2011/08/07	Khamir	TG (4.5)	2009/08/07	2009/09/11
Bushehr	AWAC (25)	2010/06/15	2011/07/26	Pohl	TG (5.8)	2009/08/07	2010/08/15
Lavar	TG (3)	2010/06/24	2011/08/19	Kaveh	AWAC (10)	2013/06/16	2013/06/30
Lavar	AWAC (25)	2010/08/02	2011/07/19	Dargahan	TG (7)	2009/08/08	2009/09/15
Dayyer	TG (3)	2008/08/23	2009/09/21	Shahid Rajaee	TG (5.2)	2009/08/08	2010/02/01
Kangan	AWAC (22)	2008/08/23	2009/09/25	Bahman	TG (3.5)	2009/10/21	2009/12/28
Taheri	TG (3)	2008/08/23	2009/09/21	Larak Island	TG (3)	2009/08/09	2010/08/14
Nayband	TG (3)	2008/08/23	2009/09/21	Larak Island	AWAC (25)	2009/10/06	201/10/12
Lavan Island	AWAC (25)	2009/08/12	2010/07/08	Sirik	TG (5.8)	2009/08/10	2010/09/04
Chiruyeh	TG (5)	2009/08/06	2010/08/18				

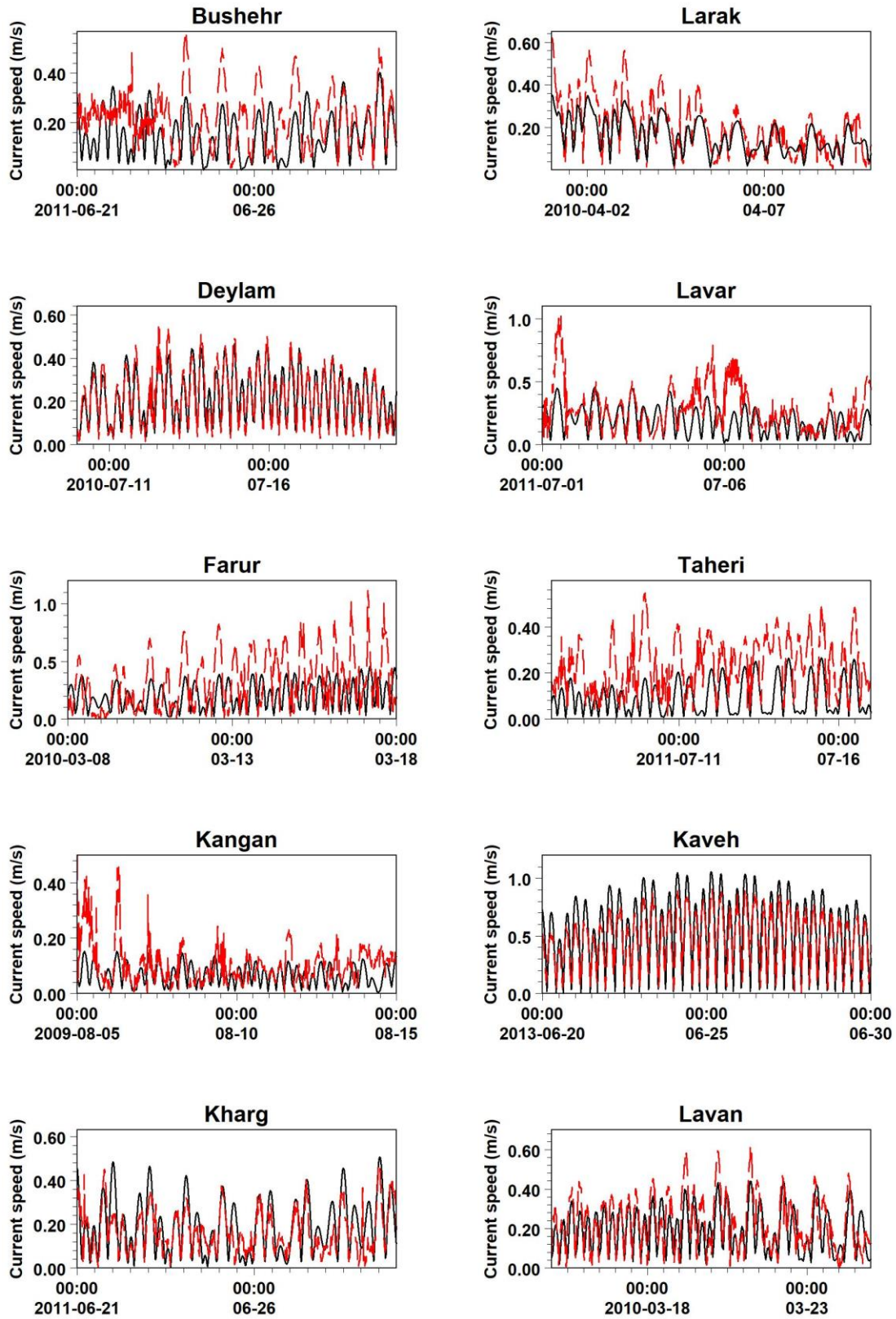


Figure R1: Comparison of the simulated (solid-line) and measured (dash-line) current speeds.

Some figures lack units on the y axis (Fig 8 and Fig. 11) and others would have increased readability with a larger font.

Thank you for the comment. Fig. 8 was corrected and Fig. 11 was modified (Please check Fig. R3 and Fig. R11).

The authors say that they select Jask-Almasnaeh as the open boundary. This is the larger domain of the two that they have. However, in figures 12-17 they present results for the small domain, in Fig 21-22 they present the results for the large domain, and again in Fig. 23-24 and 27-28 they present the small domain.

Thank you for pointing out this mistake. The location of the open boundary was chosen in the Gulf of Oman (Jask-Almasnaeh) but we cropped the maps and presented the results in the PG. The model was stable near the open boundary and its general performance can be viewed from the uploaded animation as a supplement.

We will modify Figures 21 and 22, which present the large domain, in the revised paper (Please check Fig. R8).

L110-117 and table 2 I do not think this is necessary in the introduction.

This was also a comment of the respected topic editor during the initial review process. However, it might be better to keep Table 2 and related sentences as some of the constituents have been classified in Table 5, to study the resonance period.

L130 “The mangrove forests and salt marshes at the Khuran Channel, located north of Qeshm Island, are excluded from the computational domain to improve the modeling results” I do not understand how excluding them can improve the results, do you mean you do not consider a different friction there? Is this land? Also because afterwards in L137 the manuscript reads “the grid points is also increased near mangrove locations in the Khuran Channel.”

The performance of the model was tested in both cases, i.e. with and without the Mangroves and the results of excluding them was more realistic. This might be related to the wet and drying algorithm of the employed model for the simulation of complex hydrodynamics of Mangrove forests.

Fig. 6, 18, 19, 21, 22 and fig.23, 24,27 and 28 Please change the jet color scheme and a divergent colour scheme helps understanding when negative and positive values in the same figure and so increases and decreases. Jet rainbow colour schemes can distort perceptions of data and alter meaning since they create false boundaries between values (e.g. Thyng et al (2007))

Thank you very much for your suggestion. Color schemes of the mentioned figures will be changed by a divergent color scheme entitled 'balance' from cmocean package. Please check the below Figs. R12 and R13 as well as Figs. R8 to R10.

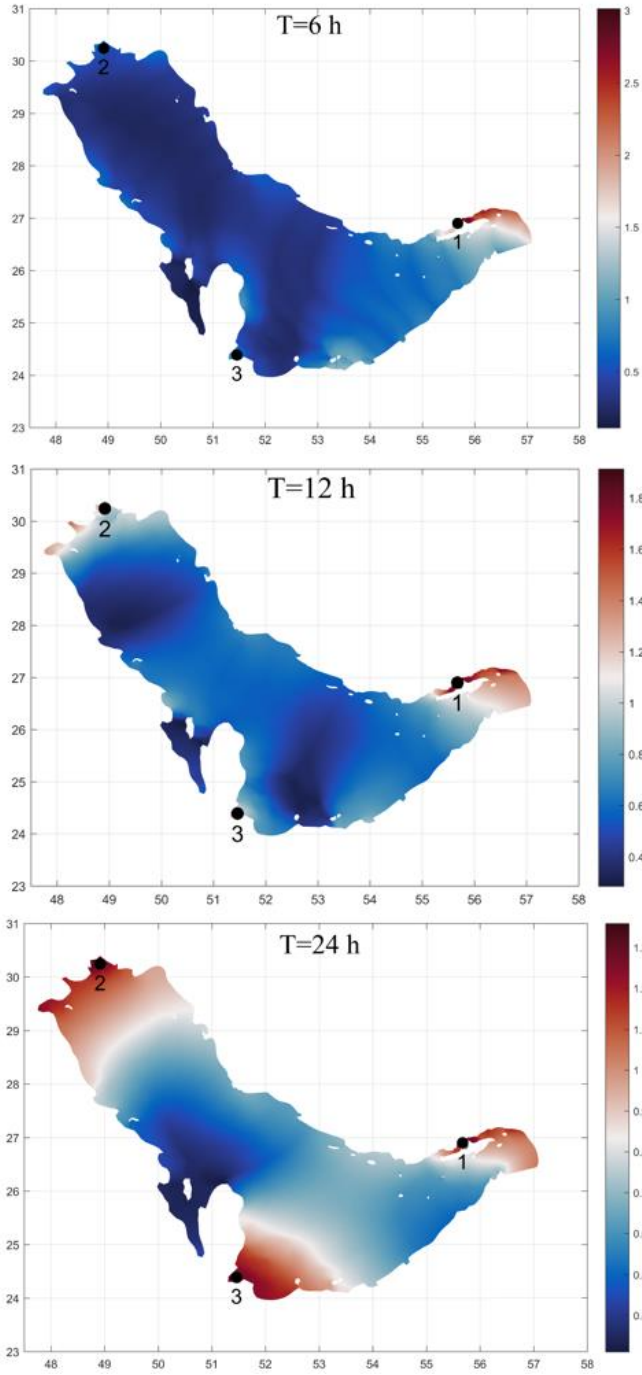


Fig. R12: The tidal amplification factors for the wave periods of 6 h (up), 12 h (middle) and 24 h (bottom).

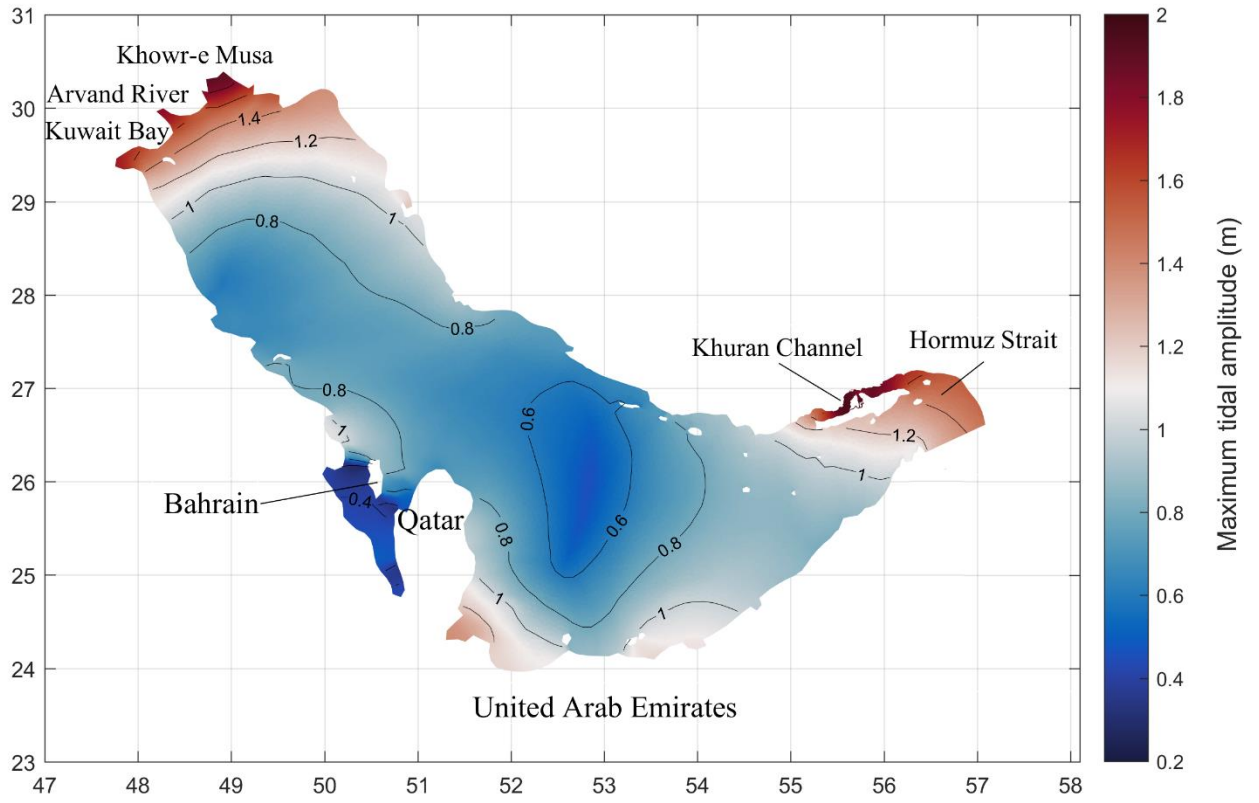


Fig. R13: Maximum tidal amplitude.

L150-151 “Although the differences of statistical measures are not significant, it is observed that all three indices correspond to the optimum Manning number of $60\text{m}^{1/3}/\text{s}$ ” This sentence needs reformulating, it is not clear what the authors mean. And the authors should also indicate what the underlined values in the table mean.

Thank you for pointing this out. The manuscript will be modified as follows (page 10, line 150):

The underlined values in columns correspond to the optimum value of the statistical indices in the stations. Although the differences of statistical measures are not significant, it is observed that Manning coefficient of $60\text{ m}^{1/3}\text{ s}^{-1}$ results to the highest degree of correlation between the model outputs and measurements.

L180, L189, L417 Please avoid using good when assessing the model those are subjective terms. The model is satisfactory for the purpose of the study or it is not.

The word “good” will be replaced by “satisfactory” in the revised manuscript.

L243 “It is also observed that the map fully conforms to the contribution of shallow-water constituents in Fig. 4. As an example, because of the decrease of water depth the contribution of shallow-water constituents increase from 3.3% to 8.9% from Larak to Pohl stations.” Not sure to what the authors refer to here, Fig4 shows the contribution of tidal constituents on the northern coastline. It is not clear how figure 4 was obtained and except for Pohl station, there are no stations on Fig. 4 on areas where the amplitude of shallow water constituents is high.

As it was also discussed above, Fig. 4 was extracted from the existing field measurements. The sentence indicates to an example where moving from Larak station towards Pohl station, the percentage of shallow-water constituents increase due to the decrease of water depth.

L 264-270 Please reformulate, I do not follow the reasoning in this paragraph. How are the checkpoints chosen?

The checkpoints were chosen in the areas where higher amplification factor were observed, i.e., Strait of Hormuz and Khuran Channel, northwest of the PG, and southeast of Qatar.

To clarify the meaning, the sentence is modified and it is moved to the previous paragraph (line 21, page 264):

Defining three numerical stations in the areas with highest amplification factors (1, 2, and 3 in Fig. 18), Table 5 presents the results of all modeled scenarios.

L 285-291 It is not clear for the second and third model whether there is Coriolis forcing or not. Why is 36m the depth chosen? From text later on, I understand this value of 36m is the average depth of the PG, but this could be presented here already.

Thank you for the comment. To clarify this, the paragraph will be modified in the revised manuscript (page 24, line 289-291):

In the second case, a horizontal flat bed with constant water depth of 36 m (=average depth of the PG) is assumed as the bathymetry of the PG. The constant water depth is also used in the third numerical test with the Manning coefficient of $0.002 \text{ s m}^{-1/3}$, i.e., the smallest value that does not make the model unstable, to concentrate on the effect of bottom friction. The Coriolis force is also included in the second and third numerical tests.

L294-315 provide theoretical information about the development of amphidromic points when bathymetry and influence of Coriolis constrained. However, the information is not presented in relation to the present study.

The theoretical information was later used for the calculations of amphidromic points in Table 6. Please kindly refer to lines 322-332.

L426-428 I understood from the description that the bathymetry was considered constant in the second test while the authors refer here to a transverse step that is not shown in the results of the numerical model. A transverse step is shown in Fig. 25 however it is not clear how this figure is produced.

Figure 25 schematically presents the response of a hypothetical gulf, where its bathymetry somehow resembles the PG, to the incoming tide. Thus, the results of the numerical tests, which are simplified cases with a hypothetical bathymetry of constant water depth, can be compared to the outputs of original model, to study the effect of different governing factors. As an example, the comparison between the results of the second test and the original model partially shows the effect of transverse step in the bathymetry (L426-428).